ORNL/TM-2023/3059

Qualification of Commercially Available Silicon Carbide for Passive Thermometry in Reactor Experiments – FY23 Status Report

Padhraic L. Mulligan
Anne A. Campbell
Chad M. Parish
Adrian M. Schrell
Benjamin La Riviere

August 2023

OAK RIDGE National Laboratory

ORNL IS MANAGED BY UT-BATTELLE LLC FOR THE US DEPARTMENT OF ENERGY

ORNL/TM-2023/3059

Nuclear Energy and Fuel Cycle Division
Materials Science and Technology Division

QUALIFICATION OF COMMERCIALLY AVAILABLE SILICON CARBIDE FOR PASSIVE THERMOMETRY IN REACTOR EXPERIMENTS – FY23 STATUS REPORT

Padhraic L. Mulligan
Anne A. Campbell
Chad M. Parish
Adrian M. Schrell
Benjamin La Riviere

August 2023

Prepared by
OAK RIDGE NATIONAL LABORATORY
Oak Ridge, TN 37831
managed by
UT-BATTELLE LLC
for the
US DEPARTMENT OF ENERGY
under contract DE-AC05-00OR22725

TABLE OF CONTENTS

LIST OF FIGURES

LIST OF TABLES

ABSTRACT

Silicon carbide (SiC) is often used as a passive temperature indicator for uninstrumented in-core nuclear experiments. For the past several decades, Oak Ridge National Laboratory has relied primarily on SiC thermometry manufactured by Dow Chemical Company, formerly Rohm and Haas because of the material's high density and reduced grain boundary elements. Although Dow SiC has performed well in this application, this material is no longer commercially available, and a new supplier is needed for future experiments. To determine a suitable replacement, a study was initiated on five types of SiC from four commercial vendors. Several critical properties, including density, electrical resistivity, chemical purity, grain structure, crystal structure, and strength were measured in samples from each material. Additionally, thermometry specimens were manufactured for irradiation in the High Flux Isotope Reactor at nominal temperatures of 300°C, 600°C, and 900°C, which will be measured using continuous dilatometry at a later date. This report provides an update of commercially available SiC material characterization and the irradiation capsule design.

1. INTRODUCTION

Silicon carbide (SiC) is a robust ceramic material suitable for use in a variety of harsh environments. Properties of SiC have been extensively studied and reviewed for a number of nuclear applications, including for tristructural isotropic (TRISO)–coated gas-reactor fuel particles [1], accident-tolerant cladding [2], and in-core instrumentation [3]. SiC can also be used as a passive thermometry in nuclear experiments, as was first proposed by Pravdyuk et al. [4] in 1960 using 6H SiC, and expanded upon further by Thorne et al. [5]. SiC operates as a passive thermometry indicator through the processes of defect accumulation. Neutron-induced point defects are formed in the SiC material over the course of an irradiation experiment. Depending on the temperature of the SiC specimen, certain defects are annealed in the specimen, while other defects that are stable above the specimen irradiation temperature continue to accumulate. By performing continuous dilatometry following irradiation [6, 7], the average experimental temperature can be determined by identifying changes in the instantaneous coefficient of thermal expansion during heating and cooling cycles.

Beta-phase (3C) SiC grown via chemical vapor deposition (CVD) is the most frequently used polytype for SiC thermometry. The phase and composition purity, as well as the mechanical integrity (i.e., density, strength, and elastic modulus) are critical properties to ensure that the SiC thermometry performs as expected. Many large irradiation campaigns depend on accurate temperature measurements using SiC to achieve a high degree of certainty in experimental conditions to meet rigorous quality control standards for licensing as well as scientific and applied research purposes.

Over the past 10–15 years, irradiation programs at Oak Ridge National Laboratory have relied on high-purity, high-resistivity β-phase SiC produced by Dow chemical, previously Rohm & Haas. Although this material has performed well historically, Dow no longer produces SiC, and new material suppliers must be qualified to support future irradiation experiments. To qualify new SiC material, a study was initiated comparing existing Dow material against SiC produced by three different suppliers: Advanced Silicon Carbide Manufacturers (ASCM), CoorsTek, and MSE Supplies. In this study, critical material properties of SiC produced by these manufactures are being investigated, including the following:

- Material phase purity, including secondary phases (Si and C) and hexagonal SiC polytypes using x-ray diffraction (XRD) phase analysis and electron backscatter diffraction (EBSD).
- Elemental impurities in SiC, particularly neighboring elements such as B, Al, and P.
- SiC grain boundaries, precipitates, and defects using transmission electron microscopy (TEM).
- Passive thermometry testing in the High Flux Isotope Reactor (HFIR) [8] at three temperatures (300, 600, 900°C) and for two irradiation cycles with subsequent continuous dilatometry measurements.

This report provides a status update of work performed in fiscal year 2023, including SiC properties measured from the samples, details of the irradiation capsule design, and planned analyses.

2. SIC MATERIALS

SiC materials were chosen from several available commercial vendors. Each material was designated an identification prefix, given in Table 1. Material A was provided by MSE and was an N-type 4H-SiC in wafer form grown by an unnamed vendor. Material B was also a SiC wafer provided by MSE and was a semi-insulating 4H-SiC material, also grown by an unnamed vendor. Material C was the historically used high-resistivity 3C material produced in plate form by Dow. Material D was high-resistivity 3C material in plate form produced by CoorsTek Korea, and material E was high-resistivity 3C SiC produced by ASCM. Figure 1 shows sample material from each supplier.

Table 1. Overview of SiC materials included in this study.

ID Prefix	Vendor	SiC Type	Form Factor
A	MSE	4H, N-type, 4.0° off axis toward <11-20>	0.35×101 mm diameter wafer
B	MSE	4H, Semi Insulating (SI), on axis <0001>	0.5×101 mm diameter wafer
C	Dow / Rohm & Haas	3C, High Resistivity	6.35×152 mm square plate
D	CoorsTek	3C PureSiC®, High Resistivity CVD	5.0×200 mm square plate
E	ASCM	3C, High Resistivity	6.35×152 mm square plate

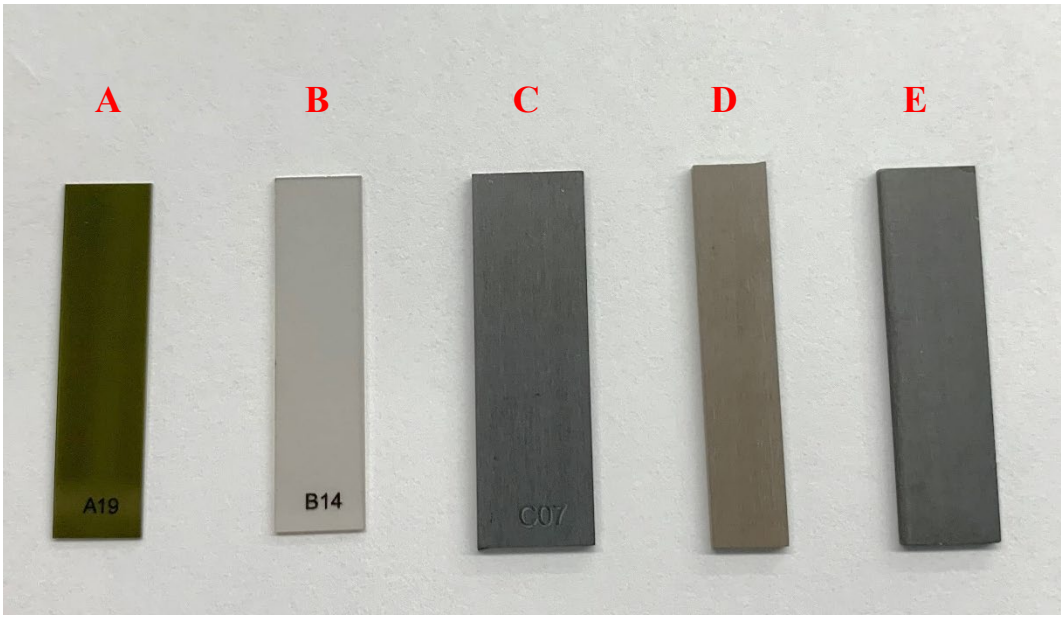

Figure 1. Samples machined from five SiC suppliers.

3. IRRADIATION CAPSULE DESIGN

Qualification of SiC materials will include irradiation of specimens at three different temperatures for two HFIR cycles, accumulating approximately 5.8 displacements per atom (dpa). Post-irradiation dilatometry on irradiated specimens will be performed to assess the suitability of each type of SiC. Design of the irradiation capsules used an existing capsule design (S17-06-CARBON03) capable of containing 16 SiC specimens, with dimensions of 6 × 24 × (0.3–0.5) mm (width, length, thickness). CAD models of the S17-06-CARBON03 rabbit capsule (Figure 2, a) were imported into ANSYS Workbench (ver. 2023 R1) for steady-state thermal analysis. Thermophysical properties and volumetric nuclear heating rates for each

material were imported into the model to determine the appropriate holder diameter and fill gas composition to achieve the desired irradiation temperatures. Material heat generation rates were referenced from existing radiation transport and depletion calculations of materials in the HFIR flux trap, which calculate heat generation rates from prompt fission neutrons, prompt fission photons, fission product decay photons, and local activation decay heat. Heat conduction though solid parts was modeled using the ANSYS thermal module, whereas heat transfer through small, unmeshed gas gaps was modeled using customized dynamic link libraries [9]. Ninety-degree (90°) symmetry simplification was used for the finite element analysis (FEA) modeling, and small rounds or fillets were removed from components for meshing, with an average mesh element size of 0.3 mm^3. 100% He capsule fill gas was used for the 300°C design, whereas 60% He–40% Ar was used for the 600°C and 900°C designs.

The outer diameter of the Mo holder was parameterized and iterated in increments of 0.01 mm for each capsule design until the average SiC specimen temperature was as close to the goal temperature as possible. Figure 2 shows the temperature distribution in the SiC for the 600°C design. The temperatures of specimens near the radial center of the rabbit capsule were higher than those of specimens located on the periphery. Also, the average temperature of specimens located at the top of the rabbit (i.e., right side of Figure 2, b) was found to be ~2% higher than that of specimens in the same radial position at the bottom of the rabbit. This higher temperature is caused by contact with the lower Mo disk and centering thimble, which provides a better heat conduction path to the capsule housing. Additionally, specimens located at the bottom of the capsule showed a greater spread of minimum and maximum temperature due to this effect. Results for the 300°C and 900°C designs also showed a similar trend. Table 2 lists the characteristics for each capsule design that will be used in the actual irradiation, whereas Figure 3 shows the minimum, maximum, and average temperature for each specimen. All capsules were designed for insertion in a target rod rabbit holder position 3.

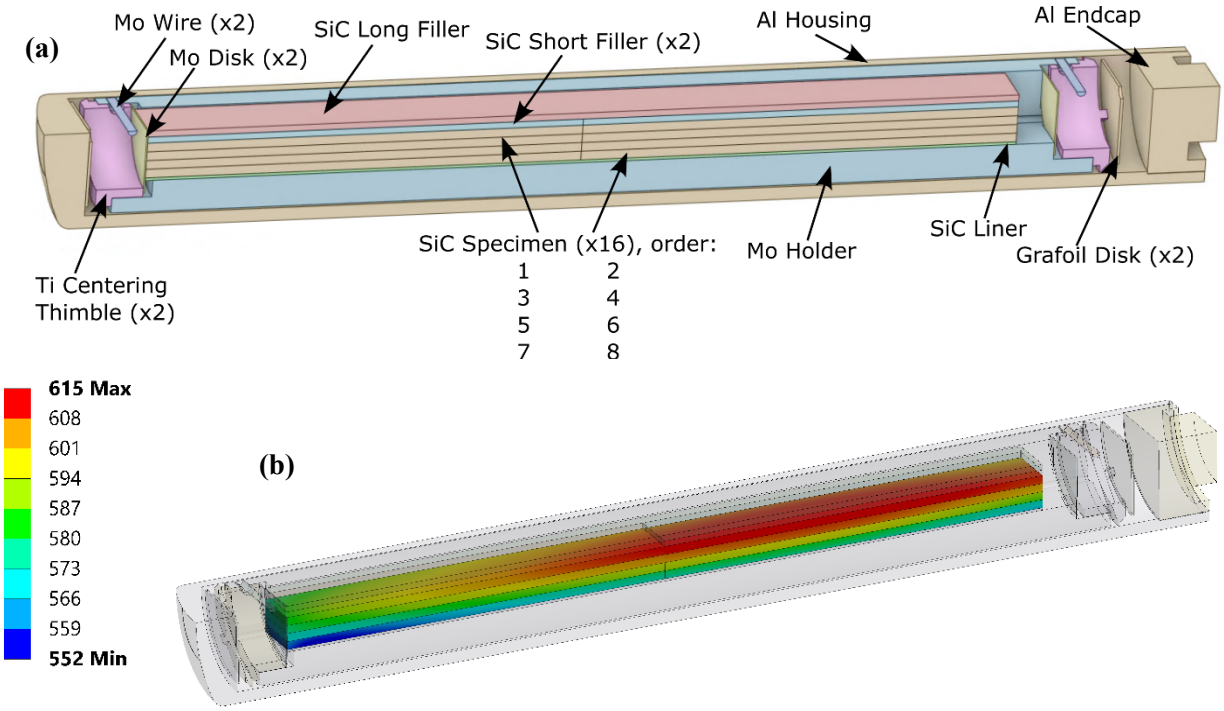

Figure 2. Components for SiC rabbit capsule with 90° symmetry (a) and SiC specimen temperatures for 600°C case (b), showing higher temperatures in rightmost specimens.

Table 2. Rabbit capsule design characteristics for TRRH position 3 and specimen average temperatures.

Target Temperature (°C)	SiC Specimen Average Temperature (°C)	Fill Gas Composition	Holder Diameter (mm)
300	303	100% He	9.40
600	590	60/40% He/Ar	9.32
900	912	60/40% He/Ar	9.04

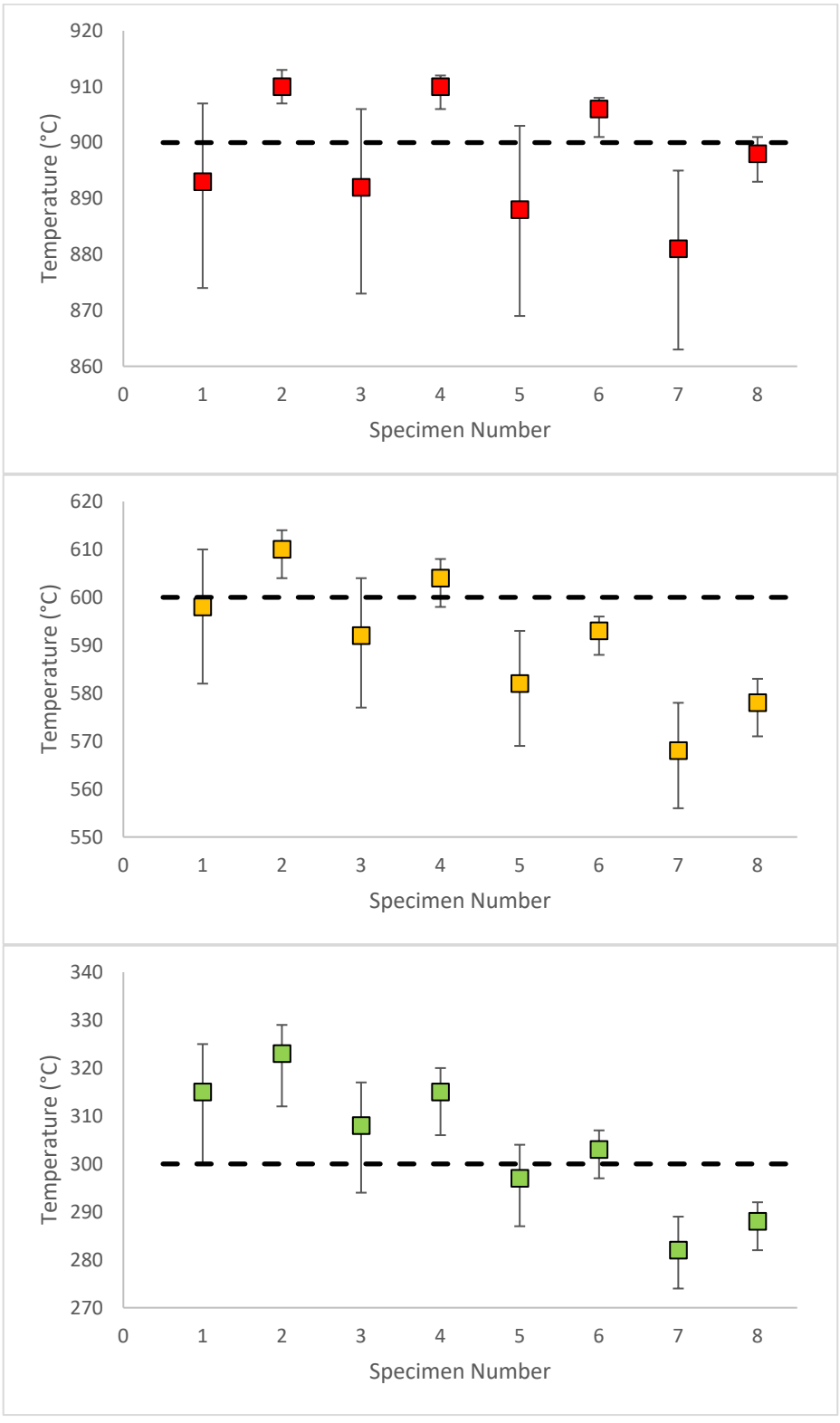

Figure 3. SiC specimen temperatures for 900°C (top), 600°C (middle), and 300°C (bottom). Markers represent specimen average temperature, and error bars correspond to minimum and maximum temperature from FEA modeling. Specimen numbers are depicted in Figure 2.

4. PRE-IRRADIATED SiC PROPERTIES

Several electronic and physical properties of the five SiC materials were characterized in the unirradiated state. Properties measured for this work are summarized in Table 3. Additional characterizations are ongoing.

Table 3. Materials properties of SiC materials or analysis methods reported in this work.

Property/Analytical Technique	SiC Material				
	A	B	C	D	E
Density	**X**	**X**	**X**		
Resistivity	**X**	**X**	**X**	**X**	**X**
Strength					
Young's Modulus	**X**	**X**	**X**		
Mass Spectrometry	**X**	**X**	**X**		
XRD					
EBSD	**X**	**X**	**X**		
TEM					

4.1 DENSITY

Density of the materials was measured via direct measurement of the parallelepiped specimen dimensions and massing of the samples. Results are reported in Table 4. Measured densities correspond well with SiC's theoretical density of 3.21 g/cm^3.

Table 4. Density of SiC materials.

	SiC Material				
	A	B	C	D	E
Specimen ID	A22	B07	C04	–	–
Density (g/cm^3)	3.17	3.21	3.21	–	–

4.2 RESISTIVITY

Bulk resistivity measurements of SiC were performed using an Ossila four-point probe system. Results are reported in Table 5. Measured resistivity values for material B, C, D, and E correspond relatively well with manufacturer stated values. The resistivity of material A was significantly higher than expected, but this finding could be caused by oxide formation on the surface.

Table 5. Resistivity of SiC materials.

	SiC Material				
	A	B	C	D	E
Specimen ID	A12	B30	C05	D01-8	E01-14
Measured Resistivity (Ω · m)	365.3 ± 2.7	> 1E4	303.1 ± 0.6	> 1E4	18.1 ± 0.4
Manufacturer Stated Resistivity (Ω · m)	0.0002	> 1E5	> 10	> 1E3	> 10

4.3 YOUNG'S MODULUS

Young's modulus was measured using the sonic resonance technique on bar specimens of SiC materials in accordance with ASTM C1198-20. The dynamic Young's modulus was calculated using

$$E = 0.9465\left(\frac{mf_f^2}{b}\right)\left(\frac{L^3}{t^3}\right)T_1, \quad (1)$$

where E is Young's modulus (Pa), m is the mass of the bar (g), f_f is the fundamental resonant frequency of the bar in flexure (Hz), and b, L, t are the width, length, and thickness of the bar (mm), respectively. Since the length to thickness ratio was >20, the T_1 correction factor was determined using a simplified formula:

$$T_1 = 1.000 + 6.585\left(\frac{t}{L}\right)^2. \quad (2)$$

Values calculated using Eq. (1) and Eq. (2) are listed in Table 6. The measured value for material A is relatively close to values for C_{11} (507 GPa) and C_{33} (547 GPa) reported by Kamitani et al. [10]. The lower modulus for material B suggests that there may be some porosity in the material [1]. The orientation of the material—4° towards <11-20> for material A and on axis <0001> for material B—may also be influencing the measurement by capturing a composite of two different crystallographic directions with lower Young's modulus, such as C_{44} (159 GPa) and C_{12} (108 GPa) [10]. The measured Young's modulus for material C is quite close to the value of 460 GPa reported in the literature [1] for polycrystalline, high-purity, dense Rohm and Haas material.

Table 6. Young's modulus of SiC materials.

	SiC Material				
	A	B	C	D	E
Specimen ID	A22	B07	C04	–	–
Young's Modulus (GPa)	540.83	448.74	471.48	–	–

4.4 MASS SPECTROMETRY

Glow discharge mass spectrometry (GDMS) was performed on each specimen using an outside vendor (Eurofins EAG) on three of the five SiC specimens, and results are listed in Table 7. Elements which appeared with different concentrations in specimens are highlighted. Boron concentrations were slightly higher in material C relative to A and B, though still in the ppm range. This result is to be expected as the primary application of material A and B is for semiconductor devices, which can be significantly impacted by the presence of boron, which acts as an acceptor within the bandgap. Nitrogen impurity concentrations could not be detected using this technique. Other elemental concentrations were relatively consistent between samples with the exception of increased Fe content in material A (N-type 4H SiC) and Na, S, and V content in material B (SI 4H SiC). Neighboring elements to Si and C (Al, P, S) appear as trace impurities in each material.

Table 7. Impurity analysis (ppm wt) for SiC samples.

Element	SiC Material (Specimen ID)			Element	SiC Material (Specimen ID)		
	A (A44)	B (B20)	C (C02)		A (A44)	B (B20)	C (C02)
Li	< 0.01	< 0.01	< 0.01	**Ag**	< 0.01	< 0.01	< 0.01
Be	< 0.01	< 0.01	< 0.01	**Cd**	< 0.1	< 0.1	< 0.1
B	0.05	0.05	1.0	**In**	Binder	Binder	Binder
C	Matrix	Matrix	Matrix	**Sn**	< 0.5	< 0.5	< 0.5
F	< 5	< 5	< 5	**Sb**	< 0.05	< 0.05	< 0.05
Na	< 0.05	0.16	< 0.05	**Te**	< 0.05	< 0.05	< 0.05
Mg	< 0.05	< 0.05	< 0.05	**I**	≤ 13	≤ 15	≤ 6
Al	< 0.05	< 0.05	< 0.05	**Cs**	< 1	< 1	< 1
Si	Matrix	Matrix	Matrix	**Ba**	< 0.05	< 0.05	< 0.05
P	< 0.05	< 0.05	< 0.05	**La**	< 1	< 1	< 1
S	0.07	0.19	0.06	**Ce**	< 0.05	< 0.05	< 0.05
Cl	0.67	0.62	0.70	**Pr**	< 0.01	< 0.01	< 0.01
K	< 0.05	< 0.05	< 0.05	**Nd**	< 0.01	< 0.01	< 0.01
Ca	< 0.05	< 0.05	< 0.05	**Sm**	< 0.01	< 0.01	< 0.01
Sc	< 0.05	< 0.05	< 0.05	**Eu**	< 0.05	< 0.05	< 0.05
Ti	< 0.01	0.01	0.01	**Gd**	< 0.01	< 0.01	< 0.01
V	< 0.005	2.7	< 0.005	**Tb**	< 0.01	< 0.01	< 0.01
Cr	< 0.5	< 0.5	< 0.5	**Dy**	< 0.01	< 0.01	< 0.01
Mn	< 0.01	< 0.01	< 0.01	**Ho**	< 0.01	< 0.01	< 0.01
Fe	0.21	0.09	0.06	**Er**	< 0.01	< 0.01	< 0.01
Co	< 0.01	< 0.01	< 0.01	**Tm**	< 0.01	< 0.01	< 0.01
Ni	< 0.05	< 0.05	< 0.05	**Yb**	< 0.01	< 0.01	< 0.01
Cu	< 0.05	< 0.05	< 0.05	**Lu**	< 0.01	< 0.01	< 0.01
Zn	< 0.05	< 0.05	< 0.05	**Hf**	< 0.01	< 0.01	< 0.01
Ga	< 0.05	< 0.05	< 0.05	**Ta**	≤ 390	≤ 460	≤ 380
Ge	< 0.05	< 0.05	< 0.05	**W**	< 0.05	< 0.05	< 0.05
As	< 0.05	< 0.05	< 0.05	**Re**	< 0.05	< 0.05	< 0.05
Se	< 0.05	< 0.05	< 0.05	**Os**	< 0.05	< 0.05	< 0.05
Br	< 0.1	< 0.1	< 0.1	**Ir**	< 0.05	< 0.05	< 0.05
Rb	< 0.05	< 0.05	< 0.05	**Pt**	< 0.05	< 0.05	< 0.05
Sr	< 0.01	< 0.01	< 0.01	**Au**	< 0.5	< 0.5	< 0.5
Y	< 0.01	< 0.01	< 0.01	**Hg**	< 0.1	< 0.1	< 0.1
Zr	< 0.01	< 0.01	< 0.01	**Tl**	< 0.01	< 0.01	< 0.01
Nb	< 0.01	< 0.01	< 0.01	**Pb**	< 0.1	< 0.1	< 0.1
Mo	< 0.05	< 0.05	< 0.05	**Bi**	< 0.01	< 0.01	< 0.01
Ru	< 0.01	< 0.01	< 0.01	**Th**	< 0.005	< 0.005	< 0.005
Rh	< 0.01	< 0.01	< 0.01	**U**	< 0.005	< 0.005	< 0.005
Pd	< 0.01	< 0.01	< 0.01				

4.5 EBSD

SiC samples from materials A, B, and C were mounted and polished metallographically using standard preparation methods. Samples were mounted in plan view (i.e., parallel to the finished surface) and in cross section. Mounted specimens were examined using Tescan MIRA3 scanning electron microscope (SEM) using the electron backscatter diffraction (EBSD) technique (Oxford Symmetry EBSD camera).

4.5.1 SiC Material A

EBSD measurements on SiC material A (Figure 4) showed high crystallinity in the 4H-SiC {0001} direction as expected, with little evidence of competing crystallographic planes.

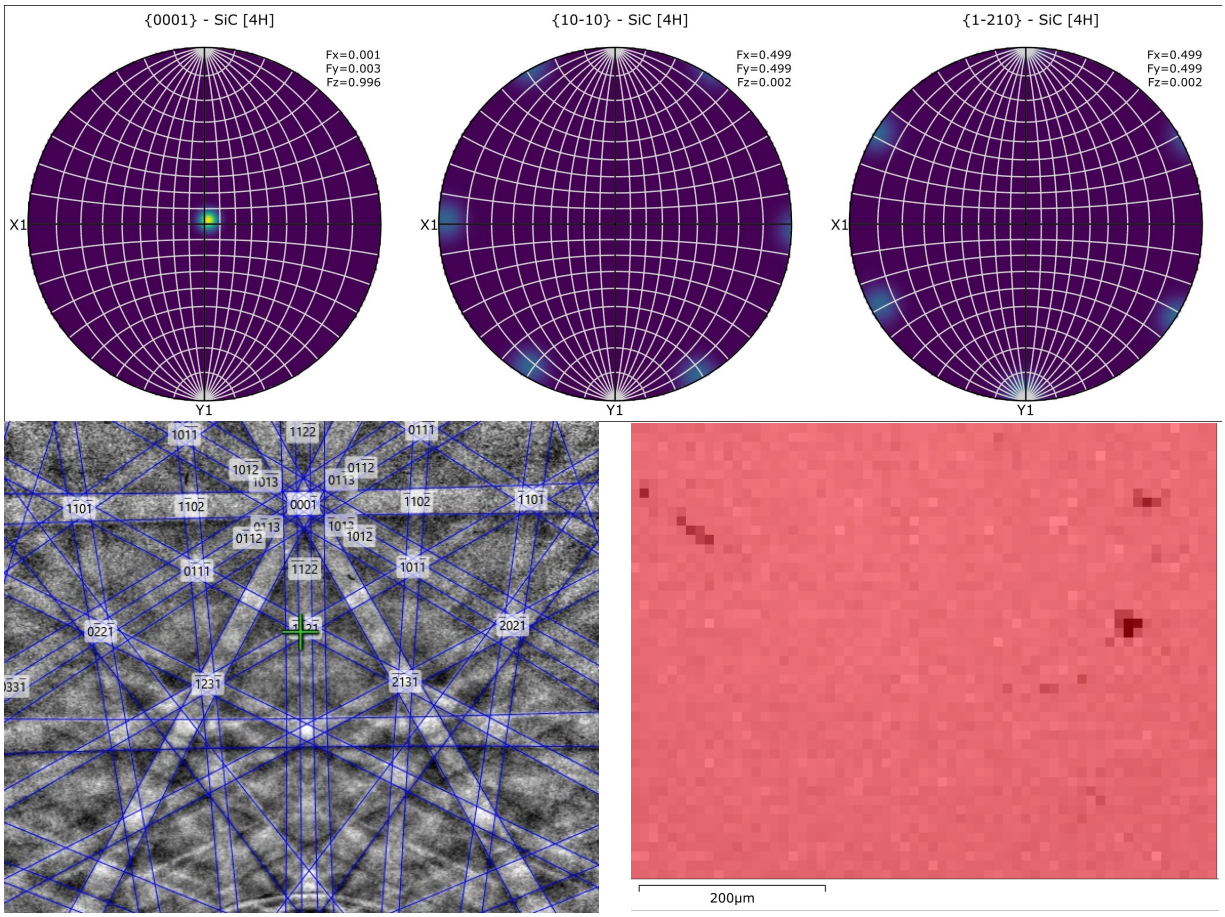

Figure 4. EBSD pole distribution maps (color scale is yellow ≈ 179 × random) for material A. Images show high crystallinity in the 4H-SiC {0001} orientation (top), EBSD pattern for 4H-SiC (lower left), and phase map with red corresponding to {0001}4H-SiC (lower right).

4.5.2 SiC Material B

SEM analysis on SiC material B (semi insulating 4H SiC) resulting in charging consistent with an insulator and required carbon coating for SEM measurements. EBSD patterns (Figure 5) for these specimens showed similar results to material A, with 4H-SiC {0001} orientation.

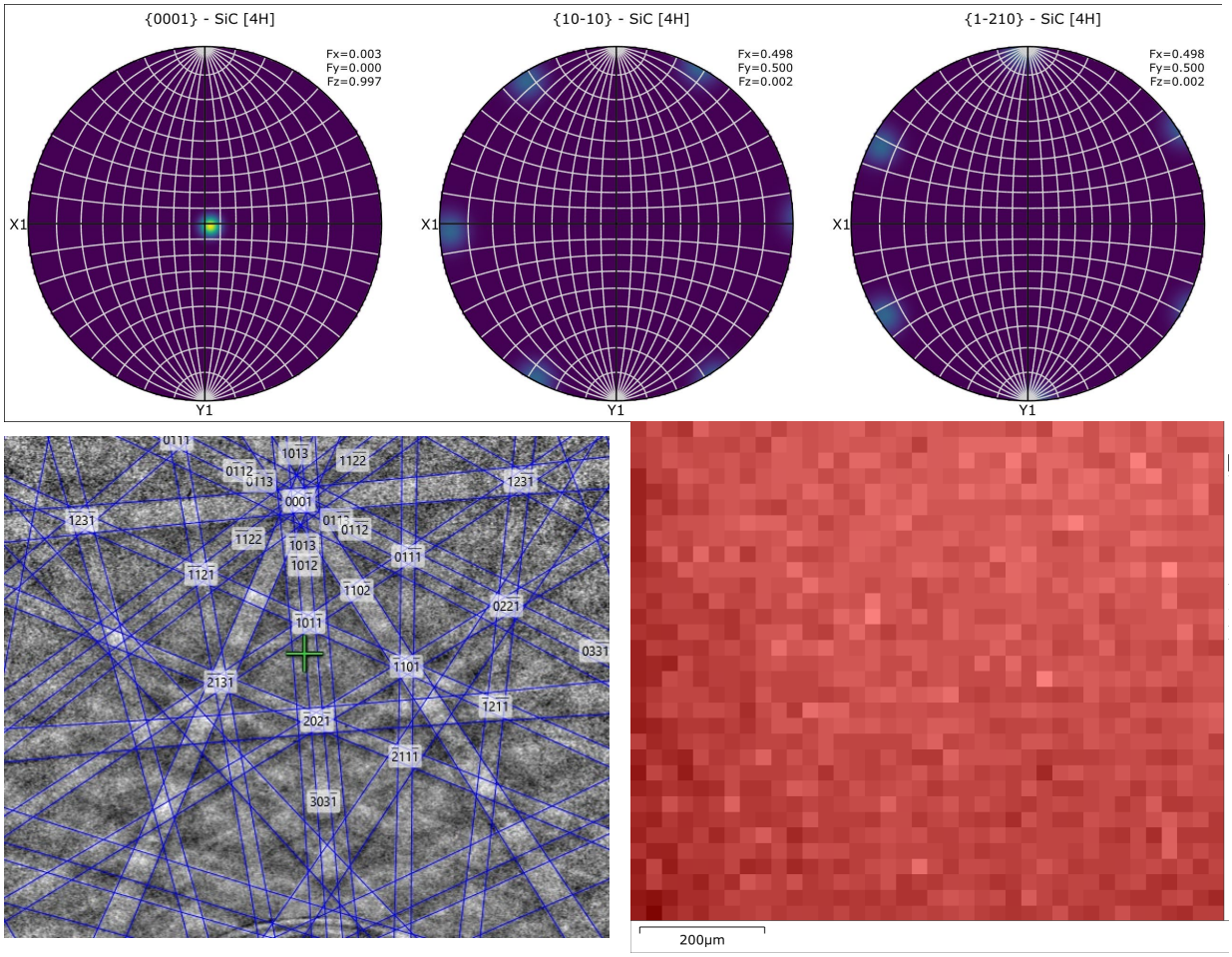

Figure 5. EBSD pole distribution maps (color scale is yellow ≈ 180 × random) for material B. Images show high crystallinity in the 4H-SiC {0001}orientation (top), EBSD pattern for 4H-SiC (lower left), and phase map with red corresponding to {0001}4H-SiC (lower right).

4.5.3 SiC Material C

SiC material C was examined using backscatter electron imaging and EBSD analysis in a similar manner to the analysis of materials A and B. EBSD data were cleaned [11] using the "Wild Spike Removal" tool in the Oxford Crystal software, unless started otherwise in the figure caption.

The cross-sectional grain size distribution data set was too small for statistical assessment. However, the plan view showed a mean grain diameter of $4.1 \pm 3.1\ \mu m$, and a mean aspect ratio of 2.6 ± 1.4. The grain sizes, however, are highly polydisperse, and the standard deviations do not do justice to the distribution; a small number of very large grains filled most of the area.

Pole figure calculations indicated a random distribution of grain orientations, with no discernable preferred orientation. The textures were dominated by the occasional very large, randomly orientated grains rather than by a growth preferred orientation.

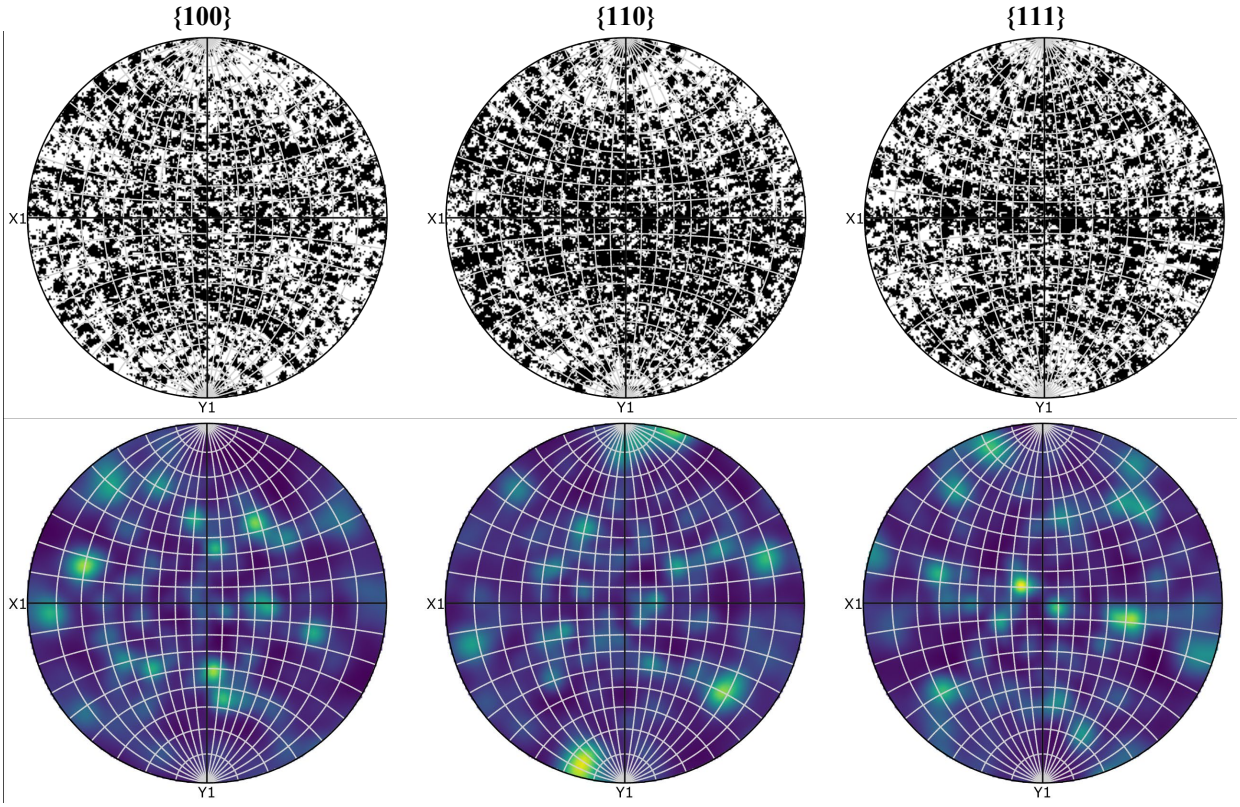

Figure 6. EBSD pole figures for cross-sectional view of material C.
Color scale correspond to yellow ≈ 4.8 × random.

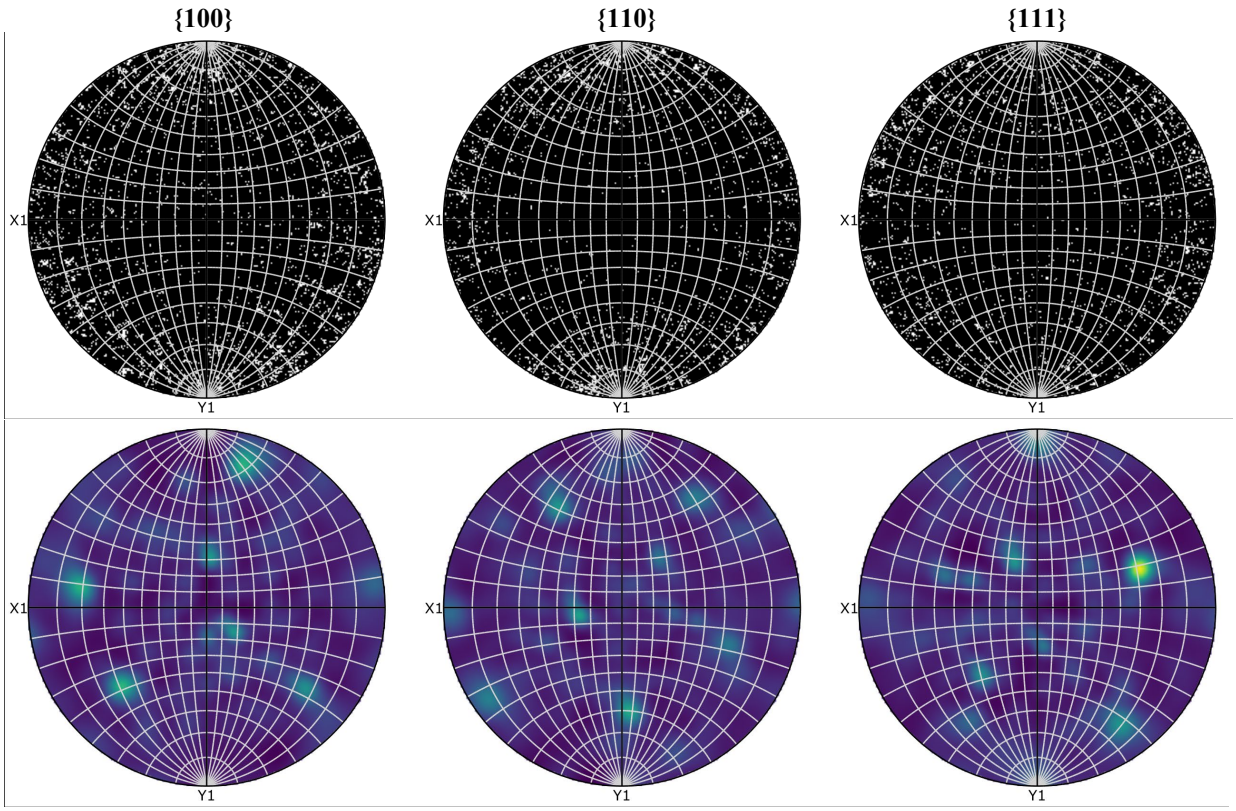

Figure 7. EBSD pole figures for plan view of material C.
Color scale corresponds to yellow ≈ 3.9 × random.

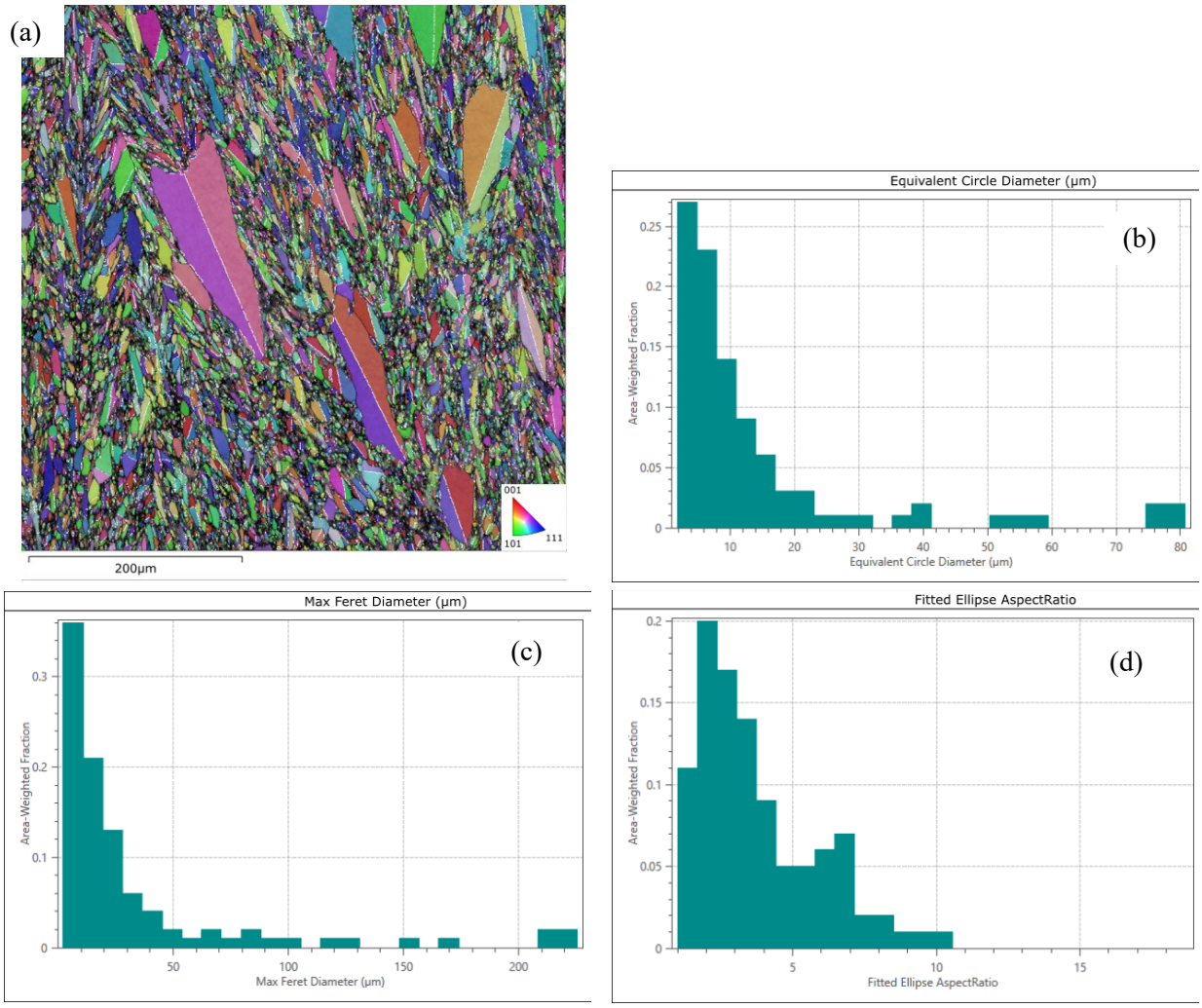

Figure 8. EBSD map (unfiltered) of plan view for material C (a) and grain size distribution for equivalent circle diameter (b), max ferret diameter (c), and aspect ratio (d). Data for grain distributions were filtered using the wild spike removal tool and five-nearest-neighbor interpolation (×2).

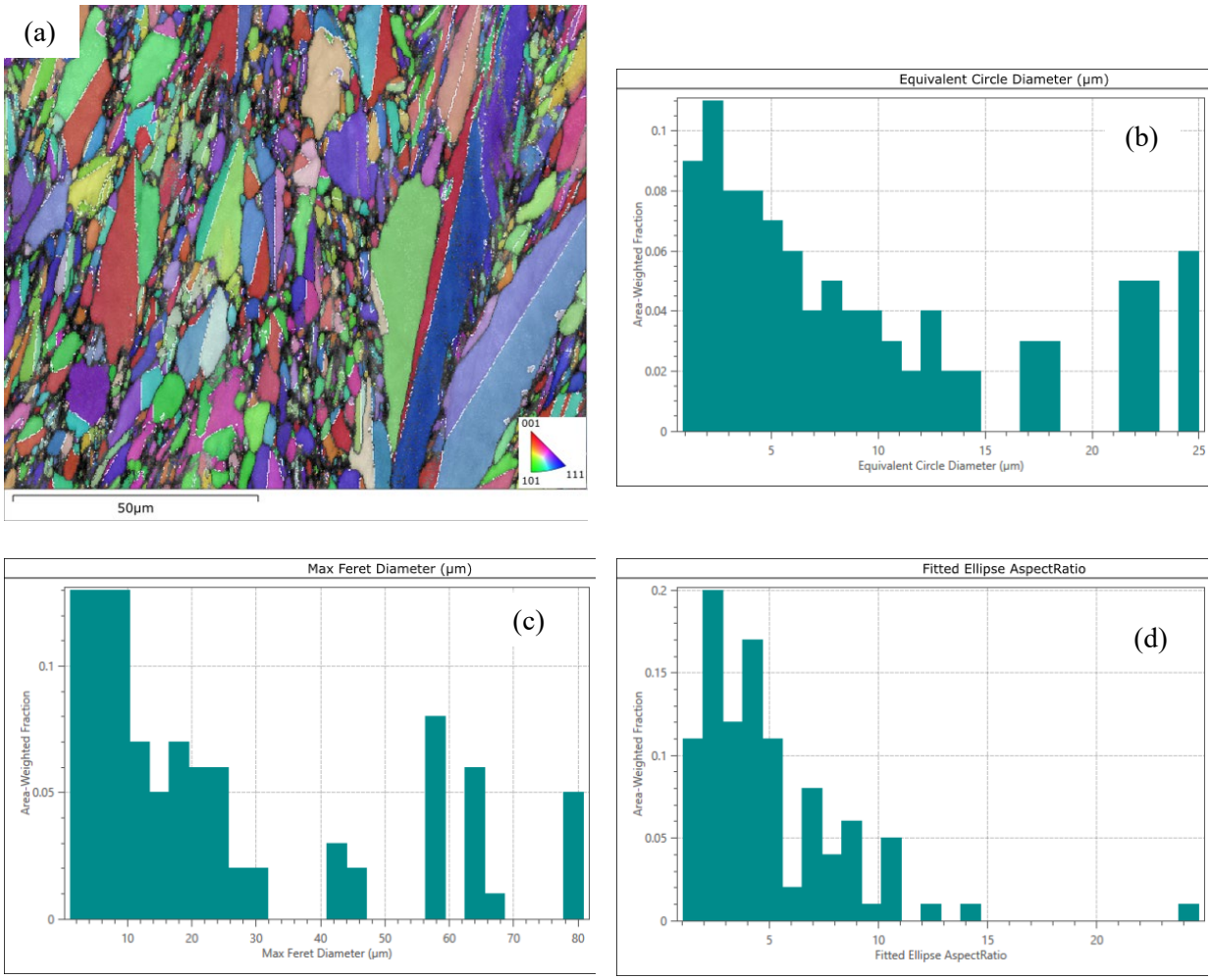

Figure 9. EBSD of cross-sectional view for material C (a) and grain size distribution for equivalent circle diameter (b), max ferret diameter (c), and aspect ratio (d). Data for grain distributions were filtered using the wild spike removal tool and five-nearest-neighbor interpolation (×2).

5. FUTURE WORK

Capsule support components (holders, housings, centering thimbles, liners, etc.) along with specimens from SiC materials A, B, and C have been received and are ready for irradiation capsule assembly. Procurement delays in specimens of materials D and E have extended analysis and irradiation of all specimens into fiscal year 2024. Remaining analyses of all materials are expected to conclude in early FY24, and irradiation is expected to take place shortly thereafter. Dilatometry on irradiated specimens is expected to occur in early 2024.

6. CONCLUSIONS

SiC is a critical material for use as a passive temperature indicator for uninstrumented in-core nuclear experiments. For the past several decades, ORNL has relied primarily on SiC thermometry manufactured by Dow Chemical Company, however, this material is no longer commercially available and a new supplier in required for future experiments. To determine a suitable replacement, a study was conducted on five types of SiC from four commercial vendors. Several critical properties, including density, electrical resistivity, chemical purity, and grain structure were measured in samples from each. Additionally, thermometry specimens were manufactured for irradiation in HFIR at nominal temperatures of 300°C, 600°C, and 900°C, which will be measured using continuously dilatometry at a later date. This report provided updates of commercially available SiC material characterization and the irradiation capsule design.

7. ACKNOWLEDGMENTS

Research performed at Oak Ridge National Laboratory was supported by the US Department of Energy Office of Nuclear Energy's (DOE NE's) Advanced Low Enriched Uranium (aLEU) program under contract no. DE-AC05–00OR22725 with UT Battelle, LLC. The authors would like to thank Ercan Carmac, Kevin Lester, Annabelle LeCoq, Stephanie Curlin for their assistance in performing this work, as well as John Batson III and Brandon Wilson for reviewing this report.

REFERENCES

1. L.L. Snead, T. Nozawa, Y. Katoh, T.-S. Byun, S. Kondo, and D.A. Petti, *Handbook of SiC Properties for Fuel Performance Modeling.* Journal of Nuclear Materials. **371**(1): p. 329-377 (2007).
2. C.P. Deck, G.M. Jacobsen, J. Sheeder, O. Gutierrez, J. Zhang, J. Stone, H.E. Khalifa, and C.A. Back, *Characterization of SiC–SiC composites for accident tolerant fuel cladding.* Journal of Nuclear Materials. **466**: p. 667-681 (2015).
3. F.B. McLean, J.M. McGarrity, C.J. Scozzie, C.W. Tipton, and W.M. DeLancey, *Analysis of neutron damage in high-temperature silicon carbide JFETs.* IEEE Transactions on Nuclear Science. **41**(6): p. 1884-1894 (1994).
4. N. Pravdyuk, V. Nikolaenko, V. Karpuchin, and V. Kuznetsov. *Investigation of diamond and silicon carbide as indicators of irradiation conditions*. in *Proceedings of the International Conference Held at Berkeley Castle*. (1961).
5. R. Thorne and V. Howard. *Radiation-Induced Changes In Porous Cubic Silicon Carbide* 1967.
6. A.A. Campbell, W.D. Porter, Y. Katoh, and L.L. Snead, *Method for Analyzing Passive Silicon Carbide Thermometry with a Continuous Dilatometer to Determine Irradiation Temperature.* Nuclear Instruments and Methods in Physics Research Section B: Beam Interactions with Materials and Atoms. **370**: p. 49-58 (2016).
7. K.G. Field, J.L. McDuffee, J.W. Geringer, C.M. Petrie, and Y. Katoh, *Evaluation of the Continuous Dilatometer Method of Silicon Carbide Thermometry for Passive Irradiation Temperature Determination.* Nuclear Instruments and Methods in Physics Research Section B: Beam Interactions with Materials and Atoms. **445**: p. 46-56 (2019).
8. R.D. Cheverton and T.M. Sims. *HFIR Core Nuclear Design*. 1971.
9. J.L. McDuffee. *Heat transfer through small moveable gas gaps in a multi-body system using the ANSYS finite element software*. in *ASME Summer Heat Transfer Conference*. Minneapolis, MN, United States (2013).
10. K. Kamitani, M. Grimsditch, J.C. Nipko, C.-K. Loong, M. Okada, and I. Kimura, *The elastic constants of silicon carbide: A Brillouin-scattering study of 4H and 6H SiC single crystals.* Journal of Applied Physics. **82**(6): p. 3152-3154 (1997).
11. L.N. Brewer and J.R. Michael, *Risks of "Cleaning" Electron Backscatter Diffraction Data.* Microscopy today. **18**(2): p. 10-15 (2010).